Dynamic multipolar polarizabilities and hyperpolarizabilities of the Sr lattice clock

Fang-Fei Wu,[1,4] Yong-Bo Tang ●,[2,3,*] Ting-Yun Shi,[1] and Li-Yan Tang ●[1,†]

[1]*State Key Laboratory of Magnetic Resonance and Atomic and Molecular Physics, Wuhan Institute of Physics and Mathematics, Chinese Academy of Sciences, Wuhan 430071, People's Republic of China*
[2]*College of Engineering Physics, Shenzhen Technology University, Shenzhen 518118, People's Republic of China*
[3]*College of Physics and Materials Science, Henan Normal University, Xinxiang 453007, People's Republic of China*
[4]*University of Chinese Academy of Sciences, Beijing 100049, People's Republic of China*

The progress in optical clocks with uncertainty at a level of 10^{-18} requires unprecedented precision in estimating the contributions of multipolar and higher-order effects of atom-field interactions. Current theoretical and experimental results of dynamic multipolar polarizabilities and hyperpolarizabilities at the magic wavelength for the Sr clock differ substantially. We combine the Dirac-Fock plus core polarization and relativistic configuration interaction methods to calculate dynamic multipolar polarizabilities and hyperpolarizabilities of the Sr atom. Our differential dynamic hyperpolarizability at the magic wavelength is $-2.09(43) \times 10^7$ a.u., which is consistent with existing theoretical and experimental results. Our differential multipolar polarizability is $2.68(94) \times 10^{-5}$ a.u., which validates independently the theoretical work of Porsev *et al.* [Phys. Rev. Lett. **120**, 063204 (2018)], but is different from recent measurements of Ushijima *et al.* [Phys. Rev. Lett. **121**, 263202 (2018)].

I. INTRODUCTION

The last few years have witnessed significant advances in optical clocks, which enable a wide range of applications, such as redefining units of time [1,2], testing the local Lorentz invariance [3,4], probing dark matter and dark energy [5,6], searching variations of fundamental constants [7–9], and detecting gravitational waves [10]. At present, the highest fractional accuracy of optical clocks has reached the level of 10^{-19} based on Al+ [11], while the uncertainty for the Sr [12,13] and Yb [14] optical lattice clocks has achieved an accuracy of 10^{-18} level. Aiming to develop optical clocks with uncertainty and stability below 10^{-18}, a better understanding and meticulous control of the atom-field interactions would benefit for the realization of higher-precision optical clocks.

The Stark shift as one significant source of systematic uncertainty for most clocks [12–14] is closely related to the polarizabilities and hyperpolarizabilities of clock states. Employing a magic wavelength optical lattice [15–17] can eliminate the leading-order of Stark shift, but cannot cancel the residual multipolar and higher-order Stark shifts for optical lattice clocks. At the level of 10^{-19} accuracy, the effects on the systematic uncertainty of optical clocks from the multipolar and higher-order atom-field interaction need to be quantitatively evaluated [18–21].

For the Sr clock, the differential dynamic multipolar polarizability of $\Delta\alpha^{QM}(\omega)$ at the magic wavelength has contra-dictions among available theoretical and experimental results. The latest measurement is $-8.01(33) \times 10^{-5}$ a.u. [21], which disagrees with the recent theoretical result of $2.80(36) \times 10^{-5}$ a.u. [20] and the previous experimental value of $0.0(2.6) \times 10^{-5}$ a.u. [22]. Especially, the signs in $\Delta\alpha^{QM}(\omega)$ between the measurement [21] and theory [20] are opposite each other. In addition, the differential dynamic hyperpolarizability at the magic wavelength also has discrepancies in theory and experiment. The recent RIKEN experimental result of $-2.10(7) \times 10^7$ a.u. [21] agrees well with the SYRTE measurement of $-2.01(45) \times 10^7$ a.u. [22,23] and the theoretical calculation of $-1.5(4) \times 10^7$ a.u. [20] but it is inconsistent with the measured value of $-1.3(1.3) \times 10^7$ a.u. in JILA [12], which is compatible with zero. Especially, the single-electron approximated result of -3.74×10^7 a.u. [19] is not within the error bar of any other existing theoretical and experimental results. Therefore, carrying out an independent theoretical calculation is expected to solve these discrepancies.

In this paper, we combine the Dirac-Fock plus core polarization (DFCP) and relativistic configuration interaction (RCI) approaches for the relativistic calculation of the divalent atoms and apply it to calculate the dynamic multipolar polarizabilities and hyperpolarizabilities at the magic wavelength for the Sr clock states by employing the sum-over-states method. The detailed comparisons for the energies, reduced matrix elements, and static dipole polarizabilities between our results and other published literature are also made. Our work not only presents an independent test for the previous calculations of Ref. [20], but also would stimulate further investigations on the differential multipolar polarizability of the Sr clock. The atomic units (a.u.) are used throughout this work except where specifically mentioned.

*ybtang@htu.edu.cn
†lytang@wipm.ac.cn

TABLE I. The radial cutoff parameter ρ_κ (in a.u.) for different quantum states.

$\kappa = -1$	$\kappa = 1$	$\kappa = -2$	$\kappa = 2$	$\kappa = -3$
2.02950	1.94995	1.95360	2.35035	2.36185

II. THEORETICAL FRAMEWORK

A. The combination method of DFCP and RCI

The basic strategy of the present theoretical method is that a divalent electron atom is simplified as a frozen core part and valence electron part. The calculation process can be divided into three steps. The first step is the Dirac-Fock (DF) calculation of the frozen core part to obtain the core orbital functions $\psi(\boldsymbol{r})$ [24].

The second step is to solve the following DFCP equation to obtain the single-electron wave functions $\phi(\boldsymbol{r})$:

$$h_{\text{DFCP}}(\boldsymbol{r})\phi(\boldsymbol{r}) = \varepsilon\phi(\boldsymbol{r}), \quad (1)$$

where $h_{\text{DFCP}}(\boldsymbol{r})$ represents the DFCP Hamiltonian,

$$h_{\text{DFCP}}(\boldsymbol{r}) = c\boldsymbol{\alpha} \cdot \mathbf{p} + (\beta - 1)c^2 + V_N(r) + V_{\text{core}}(r), \quad (2)$$

where $\boldsymbol{\alpha}$ and β are the 4×4 Dirac matrices, $\mathbf{p}$ is the momentum operator for the valence electron, $V_N(r)$ is the Coulomb potential between a valence electron and nucleus, $V_{\text{core}}(r)$ represents the interaction potential between core electrons and a valence electron, which is approximated as a DF potential and a semiempirical one-body core-polarization interaction potential [25],

$$V_{\text{core}}(r) = V_{\text{DF}}(r) + V_1(r), \quad (3)$$

with

$$V_1(r) = -\frac{\alpha_{\text{core}}}{2r^4}\left[1 - \exp\left(\frac{r^6}{\rho_\kappa^6}\right)\right], \quad (4)$$

where $\alpha_{\text{core}} = 5.812$ a.u. [26] is the static dipole polarizability of the Sr^{2+} core. ρ_κ is the radial cutoff parameter which is tuned to reproduce the experimental binding energy [27] of the lowest state of each κ angular quantum number. The values of the cutoff parameter for different κ are listed in Table I. Each κ with six significant digits is to ensure the relative error bar between the reproduced energy and the experimental energy [27] below 10^{-6}. The effect from the parameter ρ_κ on our final calculations of the multipolar polarizabilities and hyperpolarizabilities is less than 1% if ρ_κ changed 1%. The core wave functions $\psi(\boldsymbol{r})$ obtained in the first step are used to evaluate the matrix elements of the DF potential $V_{\text{DF}}(r)$ [24].

The third step is the configuration interaction calculation of a divalent electron atom. The eigenequation can be expressed as

$$\left(\sum_i^2 h_{\text{DFCP}}(\boldsymbol{r}_i) + V_{ij}\right)|\Psi(\pi JM)\rangle = E|\Psi(\pi JM)\rangle. \quad (5)$$

The two-particle interaction potential is

$$V_{ij} = \frac{1}{r_{ij}} + V_2(r_{ij}), \quad (6)$$

TABLE II. Comparison of energy (in cm^{-1}) for some selective low-lying states.

State	Present	NIST [27]	Diff.
$5s^2\,^1S_0$	-134491.48	-134897.36	-0.301%
$5s6s\,^1S_0$	-104184.28	-104305.54	-0.116%
$5p^2\,^3P_0$	-99511.11	-99703.93	-0.193%
$5p^2\,^1S_0$	-97619.69	-97737.14	-0.120%
$5s7s\,^1S_0$	-96347.02	-96453.36	-0.110%
$5s8s\,^1S_0$	-93816.62	-93845.05	-0.030%
$5s9s\,^1S_0$	-92285.67	-92300.80	-0.016%
$5s10s\,^1S_0$	-91375.90	-91385.20	-0.010%
$5s5p\,^3P_0^o$	-120241.53	-120579.86	-0.281%
$5s6p\,^3P_0^o$	-100953.10	-101043.88	-0.090%
$4d5p\,^3P_0^o$	-97533.06	-97605.30	-0.074%
$5s7p\,^3P_0^o$	-95471.60	-95485.70	-0.015%
$5s8p\,^3P_0^o$	-93174.39	-93185.32	-0.012%
$5s9p\,^3P_0^o$	-91904.58	-91911.51	-0.008%
$5s5p\,^3P_1^o$	-120066.55	-120393.03	-0.271%
$5s5p\,^1P_1^o$	-113209.78	-113198.92	-0.010%
$5s6p\,^3P_1^o$	-100941.97	-101029.05	-0.086%
$5s6p\,^1P_1^o$	-100754.48	-100798.97	-0.044%
$4d5p\,^3D_1^o$	-98662.01	-98633.22	-0.029%
$4d5p\,^3P_1^o$	-97520.99	-97594.64	-0.075%
$5s7p\,^1P_1^o$	-95944.97	-95990.51	-0.047%
$5s5p\,^3P_2^o$	-119696.91	-119998.82	-0.252%
$4d5p\,^3F_2^o$	-101482.42	-101630.52	-0.146%
$4d5p\,^1D_2^o$	-101006.28	-101070.47	-0.064%
$5s6p\,^3P_2^o$	-100843.28	-100924.30	-0.080%
$4d5p\,^3D_2^o$	-98545.47	-98515.62	-0.030%
$4d5p\,^3P_2^o$	-97484.48	-97560.78	-0.078%
$5s4f\,^3F_2^o$	-96142.22	-96146.95	-0.005%
$5s4d\,^3D_1$	-116417.74	-116738.33	-0.275%
$5s6s\,^3S_1$	-105819.31	-105858.60	-0.037%
$5s5d\,^3D_1$	-99792.66	-99890.46	-0.098%
$5p^2\,^3P_1$	-99310.15	-99497.26	-0.188%
$5s7s\,^3S_1$	-97457.80	-97472.69	-0.015%
$5s6d\,^3D_1$	-95168.98	-95211.54	-0.045%
$5s4d\,^3D_2$	-116359.19	-116678.58	-0.274%
$5s4d\,^1D_2$	-114362.94	-114747.68	-0.335%
$5s5d\,^1D_2$	-100039.09	-100169.92	-0.131%
$5s5d\,^3D_2$	-99778.03	-99875.38	-0.097%
$5p^2\,^3P_2$	-99040.99	-99222.73	-0.183%
$5p^2\,^1D_2$	-97769.91	-97936.53	-0.170%

where the first term is the Coulomb interaction between two valence electrons and the second term is the two-body core-polarization interaction with the functional form [28,29],

$$V_2(r_{ij})$$
$$= -\frac{\alpha_{\text{core}}\boldsymbol{r}_i \cdot \boldsymbol{r}_j}{r_i^3 r_j^3}\sqrt{\left[1 - \exp\left(\frac{r_i^6}{\rho_\kappa'^6}\right)\right]\left[1 - \exp\left(\frac{r_j^6}{\rho_\kappa'^6}\right)\right]}, \quad (7)$$

TABLE III. Comparison of some reduced matrix elements (in a.u.), the fourth column is the difference between present values and the results of Ref. [37].

Transition	Present	Ref. [37]	Diff.	Others
$5s^2\,^1S_0 \rightarrow 5s5p\,^1P_1^o$	5.307	5.272	0.66%	5.248(2)[a]
$5s^2\,^1S_0 \rightarrow 5s5p\,^3P_1^o$	0.152	0.158	−3.80%	0.151(2)[b]
$5s^2\,^1S_0 \rightarrow 5s6p\,^1P_1^o$	0.235	0.281	−16.4%	0.26(2)[c]
$5s5p\,^3P_0^o \rightarrow 5s4d\,^3D_1$	2.760	2.712	1.77%	2.5(1)[d]
$5s5p\,^3P_0^o \rightarrow 5s6s\,^3S_1$	2.002	1.970	1.62%	2.03(6)[e]
$5s5p\,^3P_0^o \rightarrow 5s5d\,^3D_1$	2.457	2.460	−0.12%	2.3(1)[f]
$5s5p\,^3P_0^o \rightarrow 5p^2\,^3P_1$	2.655	2.619	1.37%	2.5(1)[f]
$5s5p\,^3P_0^o \rightarrow 5s7s\,^3S_1$	0.523	0.516	1.36%	0.61(2)[f]
$5s5p\,^3P_0^o \rightarrow 5s6d\,^3D_1$	1.167	1.161	0.52%	

[a]Reference [38].
[b]Reference [39].
[c]Reference [40].
[d]Reference [41].
[e]Reference [42].
[f]Reference [43].

where ρ'_κ is obtained by averaging two corresponding ρ_κ values of the single-electron wave functions directly, when constructing the configuration-state wave functions for the divalent atoms.

The wave function $|\Psi(\pi JM)\rangle$ with parity π, angular momentum J, and magnetic quantum number M of the system is expanded as a linear combination of the configuration-state wave functions $|\Phi_I(\sigma\pi JM)\rangle$, which are constructed by the single-electron wave functions $\phi(\boldsymbol{r})$ obtained in the second step [30,31],

$$|\Psi(\pi JM)\rangle = \sum_I C_I |\Phi_I(\sigma\pi JM)\rangle, \qquad (8)$$

where C_I and σ are the expansion coefficients and the additional quantum number to define each configuration state uniquely, respectively. Throughout the present calculations, the basis functions are constructed by using the Notre Dame basis sets [32].

B. Dynamic multipolar polarizability and hyperpolarizability

For an atom exposed under a linear polarized laser field with the laser frequency ω, the dynamic magnetic-dipole and electric-quadrupole polarizabilities for the initial state $|0\rangle \equiv |n_0, J_0 = 0\rangle$ (where n_0 represents all other quantum numbers) are written as [33]

$$\alpha^{M1}(\omega) = \frac{2}{3} \sum_n \frac{\Delta E_{n0} |\langle 0\|M1\|nJ_n\rangle|^2}{\Delta E_{n0}^2 - \omega^2}, \qquad (9)$$

$$\alpha^{E2}(\omega) = \frac{1}{30} (\alpha\omega)^2 \sum_n \frac{\Delta E_{n0} |\langle 0\|Q\|nJ_n\rangle|^2}{\Delta E_{n0}^2 - \omega^2}, \qquad (10)$$

where α is the fine structure constant, $M1$ and Q are, respectively, the magnetic-dipole and electric-quadrupole transition operators. ΔE_{n0} represents the transition energy between the initial state $|0\rangle$ and the intermediate state $|nJ_n\rangle$.

For the $J_0 = 0$ state, the dynamic hyperpolarizability $\gamma_0(\omega)$ is expressed as

$$\gamma_0(\omega) = \tfrac{1}{9}\mathcal{T}(1, 0, 1, \omega, -\omega, \omega) + \tfrac{2}{45}\mathcal{T}(1, 2, 1, \omega, -\omega, \omega), \qquad (11)$$

with $\mathcal{T}(J_a, J_b, J_c, \omega_1, \omega_2, \omega_3)$ expressed as the following general formula [34]:

$$\mathcal{T}(J_a, J_b, J_c, \omega_1, \omega_2, \omega_3) = \sum_P \left[\sum_{m_a m_b m_c}{}' \frac{\langle 0\|D^{\mu_1}\|m_a J_a\rangle \langle m_a J_a\|D^{\mu_2}\|m_b J_b\rangle \langle m_b J_b\|D^{\mu_3}\|m_c J_c\rangle \langle m_c J_c\|D^{\mu_4}\|0\rangle}{(\Delta E_{m_a 0} - \omega_\sigma)(\Delta E_{m_b 0} - \omega_1 - \omega_2)(\Delta E_{m_c 0} - \omega_1)} \right.$$
$$\left. + (-1)^{J_a + J_c + 1} \delta(J_b, J_0) \sum_{m_a}{}' \frac{\langle 0\|D^{\mu_1}\|m_a J_a\rangle \langle m_a J_a\|D^{\mu_2}\|0\rangle}{(\Delta E_{m_a 0} - \omega_\sigma)} \sum_{m_c}{}' \frac{\langle 0\|D^{\mu_3}\|m_c J_c\rangle \langle m_c J_c\|D^{\mu_4}\|0\rangle}{(\Delta E_{m_c 0} + \omega_2)(\Delta E_{m_c 0} - \omega_1)} \right], \qquad (12)$$

where D^{μ_i} is the dipole transition operator and ω_i are the frequencies of the external electric field in the three directions with $\omega_\sigma = \omega_1 + \omega_2 + \omega_3$. $\sum_P$ implies a summation over the 24 terms generated by permuting the pairs $(-\omega_\sigma/D^{\mu_1})$, (ω_1/D^{μ_2}), (ω_2/D^{μ_3}), (ω_3/D^{μ_4}), the superscripts μ_i are introduced for the purpose of labeling the permutations [34,35], and the prime over the summation means that the intermediate

state of $|m_i J_i\rangle \equiv |n_0, J_0 = 0\rangle$ $(i = a, b, c)$ should be excluded in Eq. (12).

It's noted that the relationship between our hyperpolarizability $\gamma_0(\omega)$ and the $\beta(\omega)$ of Porsev *et al.* [20] is $\gamma_0(\omega) = 4\beta(\omega)$ [36], which indicates both $\mathcal{T}(1, 0, 1, \omega, -\omega, \omega)$ and $\mathcal{T}(1, 2, 1, \omega, -\omega, \omega)$ terms in Eq. (11) are four times of $Y_{101}(\omega)$ and $Y_{121}(\omega)$ of Ref. [20], respectively. Compared

TABLE IV. Contributions to the static dipole polarizability (in a.u.) of the $5s^2\,^1S_0$ and $5s5p\,^3P_0^o$ states.

	$5s^2\,^1S_0$			$5s5p\,^3P_0^o$	
Contr.	Present	Ref. [37]	Contr.	Present	Ref. [37]
$5s5p\,^1P_1^o$	189.947	187.4	$5s4d\,^3D_1$	290.162	280.2
$5s5p\,^3P_1^o$	0.234	0.25	$5s6s\,^3S_1$	39.850	38.6
$5s6p\,^1P_1^o$	0.236	0.34	$5s5d\,^3D_1$	42.700	42.8
$4d5p\,^1P_1^o$	0.976	0.95	$5p^2\,^3P_1$	48.932	47.6
			$5s7s\,^3S_1$	1.734	1.69
			$5s6d\,^3D_1$	7.855	7.8
Tail	4.813	4.60	Tail	28.766	29.1
Valance	196.206	193.54	Valance	459.999	447.79
Core	5.812	5.29	Core	5.812	5.55
Total	202.02	198.9	Total	465.81	453.4

with the dynamic multipolar polarizabilities, the calculation of the dynamic hyperpolarizabilities using the sum-over-states method is much more challenging, since the $\mathcal{T}(J_a, J_b, J_c, \omega_1, \omega_2, \omega_3)$ term involves three summations over a large number of intermediated states. This makes it more difficult to calculate the dynamic hyperpolarizability of the clock atoms with high accuracy.

In the present paper, we perform large-scale configuration-interaction calculations by constructing sufficient configurations in an appropriate cavity to make sure the completeness of intermediate states, which guarantees the accuracy of our calculations for the dynamic multipolar polarizabilities and hyperpolarizabilities.

III. RESULTS AND DISCUSSIONS

A. Comparisons of energies, reduced matrix elements, and static dipole polarizabilities

To test the correctness and reliability of our method, we make detailed comparisons of the energies, reduced matrix elements, and static dipole polarizability in Tables II–IV

between present results and other available values. From the comparison of the energies in Table II, the biggest difference between our DFCP+RCI results and NIST energy [27] is 0.335%. From Table III, it is seen that the difference for all the reduced matrix elements between our results and the values of Ref. [37] are within 2% except the $5s^2\,^1S_0 \rightarrow 5s5p\,^3P_1^o$ and $5s^2\,^1S_0 \rightarrow 5s6p\,^1P_1^o$ transitions. And from the static electric dipole polarizability in Table IV, we can see that our values are 202.02 a.u. and 465.81 a.u. for the $5s^2\,^1S_0$ and $5s5p\,^3P_0$ clock states, respectively, which agree with the results of 198.9 a.u. and 453.4 a.u. of Safronova *et al.* [37] within 3%.

Since, in the later calculations for the dynamic multipolar polarizabilities and hyperpolarizabilities, we will replace our energies with the NIST energies [27], the error bar of our values mainly comes from reduced matrix elements. From the comparison of the reduced matrix elements in Table III, although the difference between our values and results of Ref. [37] for the $5s^2\,^1S_0 \rightarrow 5s5p\,^3P_1^o$ and $5s^2\,^1S_0 \rightarrow 5s6p\,^1P_1^o$ transitions is about -3.8% and -16.4%. However, both of them only have about 0.12% contribution to the ground-state polarizability (see from Table IV), which are much smaller than the 94% contribution from the $5s^2\,^1S_0 \rightarrow 5s5p\,^1P_1^o$ transition. This indicates that the large difference in the reduced matrix elements of $5s^2\,^1S_0 \rightarrow 5s5p\,^3P_1^o$ and $5s^2\,^1S_0 \rightarrow 5s6p\,^1P_1^o$ transitions between our values and other results has little effect on the final polarizability. Therefore, we can introduce $\pm 3\%$ fluctuation into all the reduced matrix elements to evaluate conservatively the uncertainty of our multipolar polarizabilities and hyperpolaribilities.

B. Comparison of multipolar polarizabilities

Table V lists the dynamic magnetic-dipole, electric-quadrupole polarizabilities of the $5s^2\,^1S_0$ and $5s5p\,^3P_0^o$ clock states at the 813.4280(5) nm [44] magic wavelength. A direct comparison between our work and the calculations of Porsev *et al.* [20] are also given in this table. The differential $M1$ polarizability $\Delta\alpha^{M1}(\omega)$ is determined thoroughly by $\alpha_{3P_0^o}^{M1}(\omega)$, since the $\alpha_{3P_0^o}^{M1}(\omega)$ polarizability is more than three orders of

TABLE V. The dynamic magnetic-dipole and electric-quadrupole polarizabilities (in a.u.) for the $5s^2\,^1S_0$ and $5s5p\,^3P_0^o$ clock states at the 813.4280(5) nm magic wavelength. $\Delta\alpha^{M1}(\omega) = \alpha_{3P_0^o}^{M1}(\omega) - \alpha_{1S_0}^{M1}(\omega)$ and $\Delta\alpha^{E2}(\omega) = \alpha_{3P_0^o}^{E2}(\omega) - \alpha_{1S_0}^{E2}(\omega)$ represent the difference for the clock states of the dynamic magnetic-dipole and electric-quadrupole polarizabilities, respectively, and $\Delta\alpha^{QM}(\omega) = \Delta\alpha^{M1}(\omega) + \Delta\alpha^{E2}(\omega)$. The numbers in parentheses are computational uncertainties. The numbers in the square brackets denote powers of ten.

	Present	Ref. [20]	
Polarizability	DFCP+RCI	CI+PT	CI+all-order
$\alpha_{1S_0}^{M1}(\omega)$	2.12(13)[−9]	2.19[−9]	2.37[−9]
$\alpha_{3P_0^o}^{M1}(\omega)$	−5.05(31)[−6]	−5.09[−6]	−5.08[−6]
$\Delta\alpha^{M1}(\omega)$	−5.05(31)[−6]	−5.09[−6]	−5.08[−6]
$\alpha_{1S_0}^{E2}(\omega)$	9.26(56)[−5]	8.61[−5]	8.87(26)[−5]
$\alpha_{3P_0^o}^{E2}(\omega)$	12.44(76)[−5]	12.1[−5]	12.2(25)[−5]
$\Delta\alpha^{E2}(\omega)$	3.18(94)[−5]	3.50[−5]	3.31(36)[−5]
$\Delta\alpha^{QM}(\omega)$	2.68(94)[−5]	2.99[−5]	2.80(36)[−5]

TABLE VI. The dynamic hyperpolarizabilities (in a.u.) for the $5s^2\ {}^1S_0$ and $5s5p\ {}^3P_0^o$ clock states at the 813.4280(5) nm magic wavelength. $\frac{1}{36}\mathcal{T}(1,0,1,\omega,-\omega,\omega) = \frac{1}{9}Y_{101}(\omega)$ and $\frac{1}{90}\mathcal{T}(1,2,1,\omega,-\omega,\omega) = \frac{2}{45}Y_{121}(\omega)$, where the definition of $Y_{101}(\omega)$ and $Y_{121}(\omega)$ can refer to Ref. [20]. The numbers in parentheses are computational uncertainties. The numbers in the square brackets denote powers of ten.

| Hyperpolarizability | $5s^2\ {}^1S_0$ | | | $5s5p\ {}^3P_0^o$ | | |
| | Present | Ref. [20] | | Present | Ref. [20] | |
	DFCP+RCI	CI+all-order	CI+PT	DFCP+RCI	CI+all-order	CI+PT
$\frac{1}{36}\mathcal{T}(1,0,1,\omega,-\omega,\omega)$	−6.70[5]	−6.18[5]	−6.06[5]	−7.88[6]	−7.57[6]	−7.50[6]
$\frac{1}{90}\mathcal{T}(1,2,1,\omega,-\omega,\omega)$	1.49[6]	1.41[6]	1.33[6]	−1.22[7]	−6.58[6]	−3.03[6]
Total for $\frac{1}{4}\gamma_0(\omega)$	8.20[5]	7.90[5]	7.25[5]	−2.01[7]	−1.42[7]	−1.05[7]
Recommended $\frac{1}{4}\gamma_0(\omega)$	8.2(2.0)[5]	7.90(65)[5]		−2.01(43)[7]	−1.42(37)[7]	
Recommended $\frac{1}{4}\Delta\gamma_0(\omega)$	−2.09(43)[7]	−1.5(4)[7]				

magnitude larger than $\alpha_{1S_0}^{M1}(\omega)$ polarizability. The differential $E2$ polarizability $\Delta\alpha^{E2}(\omega)$ is an order of magnitude larger than $\Delta\alpha^{M1}(\omega)$. The final value of the differential dynamic multipolar polarizability $\Delta\alpha^{QM}(\omega)$ is $2.68(94) \times 10^{-5}$ a.u., which agrees well with the CI+all-order result of $2.80(36) \times 10^{-5}$ a.u. [20].

The detailed comparison for the differential multipolar polarizability between theory and experiment is summarized in Fig. 1. It is seen that for $\Delta\alpha^{QM}(\omega)$, there are obvious differences among values of CI+all-order method [20] and the single-electron Fues′ model potential (FMP) approach [18,19]. Especially, the recent measurement in RIKEN [21] disagrees with earlier measurements of Ref. [22], and also disagrees with all the theoretical values, even the signs of $\Delta\alpha^{QM}(\omega)$ between theory and experiment are still opposite. Our work independently validates the CI+all-order calculations of Ref. [20], but differs from recent experimental measurements [21]. This existing discrepancy deserves further theoretical and experi-

mental investigations on the multipolar polarizabilities of the Sr clock.

C. Comparison of hyperpolarizabilities

The dynamic hyperpolarizabilities of the $5s^2\ {}^1S_0$ and $5s5p\ {}^3P_0^o$ clock states at 813.4280(5) nm [44] magic wavelength for the Sr atom are presented in Table VI. Since there is a factor of 4 difference in the definition of the hyperpolarizability between our $\gamma_0(\omega)$ and $\beta(\omega)$ of Porsev *et al.* [20], we use $\frac{1}{36}\mathcal{T}(1,0,1,\omega,-\omega,\omega) = \frac{1}{9}Y_{101}(\omega)$ and $\frac{1}{90}\mathcal{T}(1,2,1,\omega,-\omega,\omega) = \frac{2}{45}Y_{121}(\omega)$ to make a direct comparison with the calculations of Porsev *et al.* [20]. Our values for both terms of $\frac{1}{36}\mathcal{T}(1,0,1,\omega,-\omega,\omega)$ and $\frac{1}{90}\mathcal{T}(1,2,1,\omega,-\omega,\omega)$ are much closer to the CI+all-order values than the CI+perturbation theory (PT) results of Ref. [20]. The difference of the $\frac{1}{36}\mathcal{T}(1,0,1,\omega,-\omega,\omega)$ term for the $5s^2\ {}^1S_0$ state between present value and CI+all-order [20] value is about 8%. For the $\frac{1}{90}\mathcal{T}(1,2,1,\omega,-\omega,\omega)$
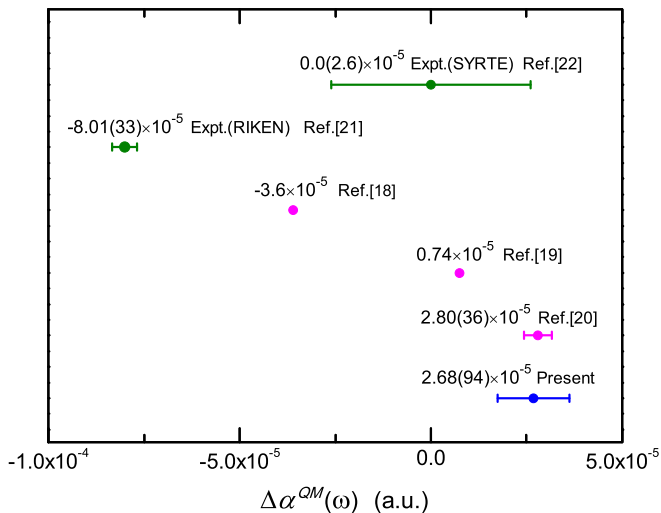

FIG. 1. Comparison of the $\Delta\alpha^{QM}(\omega)$ (in a.u.). The green line represents measurement results. The blue line represents our present value, and the magenta line denotes other theoretical results.
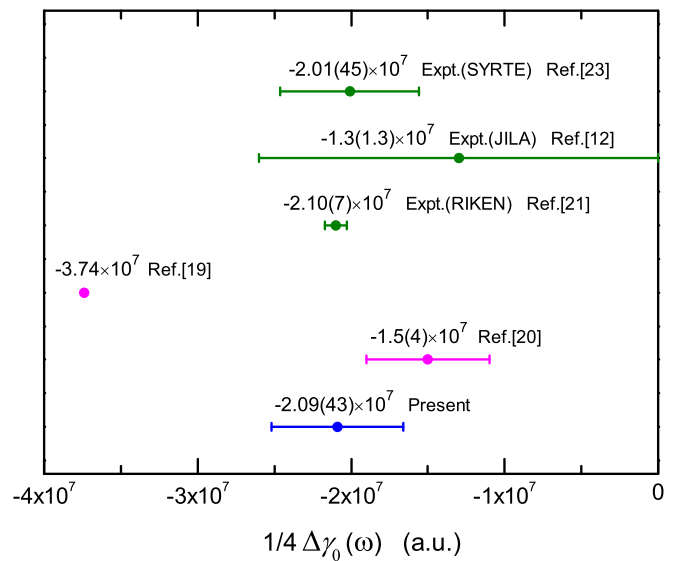

FIG. 2. Comparison of the $\frac{1}{4}\Delta\gamma_0(\omega)$ (in a.u.). The green line represents the experimental values, the blue line represents the present result, and the magenta line denotes other theoretical values.

term, the agreement between our values with the results of Ref. [20] is much better for the $5s^2\,^1S_0$ state than the $5s5p\,^3P_0^o$ state, due to the calculations of dynamic hyperpolarizability for the $5s5p\,^3P_0^o$ state involving much more intermediated states, and the completeness of intermediate states is vital for the reliability of the calculations. Our recommended values of $\frac{1}{4}\gamma_0(\omega)$ are $8.2(2.0) \times 10^5$ a.u. and $-2.01(43) \times 10^7$ a.u. for the $5s^2\,^1S_0$ and $5s5p\,^3P_0^o$ states, respectively, which agree well with the values of Ref. [20]. The final recommended value for the differential hyperpoalrizability $\frac{1}{4}\Delta\gamma_0(\omega)$ is $-2.09(43) \times 10^7$ a.u., which is mainly determined by the hyperpolarizability of the $5s5p\,^3P_0^o$ state.

The detailed comparison of the differential hyperpolarizabilitiy for the Sr atom is displayed in Fig. 2. It is seen that the FMP value of -3.74×10^7 a.u. [19] is not within the error bar of any theoretical and experimental results. Two independent theoretical results between our DFCP+RCI value $-2.09(43) \times 10^7$ a.u. and the CI+all-order result $-1.5(4) \times 10^7$ a.u. of Ref. [20] are both in good agreement with the recent high-accuracy measurement of $-2.10(7) \times 10^7$ a.u. in RIKEN [21] and $-2.01(45) \times 10^7$ a.u. in SYRTE [23].

IV. SUMMARY

We carried out the calculations of the dynamic magnetic-dipole, electric-quadrupole polarizabilities, and hyperpolarizabilities at the magic wavelength for the $5s^2\,^1S_0$ and $5s5p\,^3P_0^o$ clock states of the Sr atom by using the combined DFCP+RCI method. For the differential hyperpolarizability, our result of $-2.09(43) \times 10^7$ a.u. is in good agreement with the theoretical value of Porsev *et al.* [20] and the measurement results of Refs [21,23]. For the differential multipolar polarizability of $\Delta\alpha^{QM}(\omega)$, two independent theoretical calculations from our DFCP+RCI method and the CI+all-order approach of Porsev *et al.* [20] are consistent with each other, but both have obvious differences from recent experimental measurements [21], even the signs of the values are opposite. So, the difference about $\Delta\alpha^{QM}(\omega)$ in the Sr clock is still pending, which calls for further experimental investigation to resolve this discrepancy.

[1] F. Bregolin, G. Milani, M. Pizzocaro, B. Rauf, P. Thoumany, F. Levi, and D. Calonico, J. Phys. Conf. Ser. **841**, 012015 (2017).

[2] K. Yamanaka, N. Ohmae, I. Ushijima, M. Takamoto, and H. Katori, Phys. Rev. Lett. **114**, 230801 (2015).

[3] H. Pihan-Le Bars, C. Guerlin, R.-D. Lasseri, J.-P. Ebran, Q. G. Bailey, S. Bize, E. Khan, and P. Wolf, Phys. Rev. D **95**, 075026 (2017).

[4] R. Shaniv, R. Ozeri, M. S. Safronova, S. G. Porsev, V. A. Dzuba, V. V. Flambaum, and H. Häffner, Phys. Rev. Lett. **120**, 103202 (2018).

[5] A. Arvanitaki, J. Huang, and K. Van Tilburg, Phys. Rev. D **91**, 015015 (2015).

[6] B. M. Roberts, G. Blewitt, C. Dailey, M. Murphy, M. Pospelov, A. Rollings, J. Sherman, W. Williams, and A. Derevianko, Nat. Commun. **8**, 1195 (2017).

[7] R. M. Godun, P. B. R. Nisbet-Jones, J. M. Jones, S. A. King, L. A. M. Johnson, H. S. Margolis, K. Szymaniec, S. N. Lea, K. Bongs, and P. Gill, Phys. Rev. Lett. **113**, 210801 (2014).

[8] N. Huntemann, B. Lipphardt, C. Tamm, V. Gerginov, S. Weyers, and E. Peik, Phys. Rev. Lett. **113**, 210802 (2014).

[9] M. S. Safronova, S. G. Porsev, C. Sanner, and J. Ye, Phys. Rev. Lett. **120**, 173001 (2018).

[10] S. Kolkowitz, I. Pikovski, N. Langellier, M. D. Lukin, R. L. Walsworth, and J. Ye, Phys. Rev. D **94**, 124043 (2016).

[11] S. M. Brewer, J. S. Chen, A. M. Hankin, E. R. Clements, C. W. Chou, D. J. Wineland, D. B. Hume, and D. R. Leibrandt, Phys. Rev. Lett. **123**, 033201 (2019).

[12] T. Nicholson, S. Campbell, R. Hutson, G. Marti, B. Bloom, R. McNally, W. Zhang, M. Barrett, M. Safronova, G. Strouse *et al.*, Nat. Commun. **6**, 6896 (2015).

[13] S. L. Campbell, R. B. Hutson, G. E. Marti, A. Goban, N. Darkwah Oppong, R. L. McNally, L. Sonderhouse, J. M. Robinson, W. Zhang, B. J. Bloom *et al.*, Science **358**, 90 (2017).

[14] W. F. McGrew, X. Zhang, R. J. Fasano, S. A. Schäffer, K. Beloy, D. Nicolodi, R. C. Brown, N. Hinkley, G. Milani, M. Schioppa *et al.*, Nature **564**, 87 (2018).

[15] H. Katori, T. Ido, and M. Kuwata-Gonokami, J. Phys. Soc. Jpn. **68**, 2479 (1999).

[16] H. Katori, M. Takamoto, V. G. Pal'chikov, and V. D. Ovsiannikov, Phys. Rev. Lett. **91**, 173005 (2003).

[17] J. Ye, D. W. Vernooy, and H. J. Kimble, Phys. Rev. Lett. **83**, 4987 (1999).

[18] V. D. Ovsiannikov, V. G. Pal'chikov, A. V. Taichenachev, V. I. Yudin, and H. Katori, Phys. Rev. A **88**, 013405 (2013).

[19] H. Katori, V. D. Ovsiannikov, S. I. Marmo, and V. G. Palchikov, Phys. Rev. A **91**, 052503 (2015).

[20] S. G. Porsev, M. S. Safronova, U. I. Safronova, and M. G. Kozlov, Phys. Rev. Lett. **120**, 063204 (2018).

[21] I. Ushijima, M. Takamoto, and H. Katori, Phys. Rev. Lett. **121**, 263202 (2018).

[22] P. G. Westergaard, J. Lodewyck, L. Lorini, A. Lecallier, E. A. Burt, M. Zawada, J. Millo, and P. Lemonde, Phys. Rev. Lett. **106**, 210801 (2011).

[23] R. Le Targat, L. Lorini, Y. Le Coq, M. Zawada, J. Guéna, M. Abgrall, M. Gurov, P. Rosenbusch, D. G. Rovera, B. Nagórny *et al.*, Nat. Commun. **4**, 2109 (2013).

[24] Y.-B. Tang, C.-B. Li, and H.-X. Qiao, Chin. Phys. B **23**, 063101 (2014).

[25] J. Mitroy and D. W. Norcross, Phys. Rev. A **37**, 3755 (1988).

[26] U. I. Safronova, Phys. Rev. A **82**, 022504 (2010).

[27] A. Kramida, Y. Ralchenko, J. Reader, and NIST ASD Team, NIST Atomic Spectra Database, version 5.0.0.

[28] J. Mitroy, M. S. Safronova, and C. W. Clark, J. Phys. B **43**, 202001 (2010).

[29] J. Mitroy and M. W. J. Bromley, Phys. Rev. A **68**, 052714 (2003).

[30] M. H. Chen, K. T. Cheng, and W. R. Johnson, Phys. Rev. A **47**, 3692 (1993).

[31] Y.-H. Zhang, L.-Y. Tang, X.-Z. Zhang, and T.-Y. Shi, Phys. Rev. A **92**, 012515 (2015).

[32] W. R. Johnson, S. A. Blundell, and J. Sapirstein, Phys. Rev. A **37**, 307 (1988).

[33] S. G. Porsev, A. Derevianko, and E. N. Fortson, Phys. Rev. A **69**, 021403(R) (2004).

[34] L.-Y. Tang, Z.-C. Yan, T.-Y. Shi, and J. F. Babb, Phys. Rev. A **90**, 012524 (2014).

[35] J. Pipin and D. M. Bishop, Phys. Rev. A **45**, 2736 (1992).

[36] N. L. Manakov, V. D. Ovsiannikov, and L. P. Rapoport, Phys. Reports **141**, 320 (1986).

[37] M. S. Safronova, S. G. Porsev, U. I. Safronova, M. G. Kozlov, and C. W. Clark, Phys. Rev. A **87**, 012509 (2013).

[38] M. Yasuda, T. Kishimoto, M. Takamoto, and H. Katori, Phys. Rev. A **73**, 011403(R) (2006).

[39] R. Drozdowski, M. Ignasiuk, J. Kwela, and J. Heldt, Z. Phys. D **41**, 125 (1997).

[40] W. H. Parkinson, E. H. Reeves, and F. S. Tomkins, J. Phys. B **9**, 157 (1976).

[41] D. A. Miller, L. You, J. Cooper, and A. Gallagher, Phys. Rev. A **46**, 1303 (1992).

[42] G. Jönsson, C. Levinson, A. Persson, and C. G. Wahlström, Z. Phys. A **316**, 255 (1984).

[43] J. E. Sansonetti and G. Nave, J. Phys. Chem. Ref. Data **39**, 033103 (2010).

[44] J. Ye, H. J. Kimble, and H. Katori, Science **320**, 1734 (2008).